Appendix 6

Titus Kuehne, MD
Maythem Saeed, DVM, PhD
Phillip Moore, MD
Kelly Gleason, MD
Gautham Reddy, MD
David Teitel, MD
Charles B. Higgins, MD

Index terms:
Magnetic resonance (MR), artifact, 944.93
Magnetic resonance (MR), cine studies, 944.121419
Magnetic resonance (MR), contrast media, 944.12143
Magnetic resonance (MR), vascular studies, 944.12144
Stents and prostheses, 944.1268

Published online before print
10.1148/radiol.2232010975
Radiology 2002; 223:439–445

Abbreviations:
RF = radio frequency
SNR = signal-to-noise ratio
VEC = velocity-encoded cine

[1] From the Department of Radiology, Division of Pediatric Cardiology, University of California San Francisco, 505 Parnassus Ave, L308, San Francisco, CA 94143-0628. Received May 29, 2001; revision requested July 2; revision received September 7; accepted October 26. **Address correspondence to** C.B.H. (e-mail: *charles.higgins@radiology.ucsf.edu*).

Author contributions:
Guarantors of integrity of entire study, T.K., M.S., C.B.H., P.M.; study concepts and design, T.K., M.S., C.B.H., P.M.; literature research, T.K., M.S.; experimental studies, T.K., M.S., K.G., D.T., P.M., G.R.; data acquisition, analysis, and interpretation, T.K., M.S.; statistical analysis, T.K., M.S.; manuscript preparation, T.K., M.S.; manuscript definition of intellectual content, T.K., M.S., C.B.H.; manuscript editing, T.K., M.S., P.M., C.B.H.; manuscript revision/review, T.K., M.S.; manuscript final version approval, all authors.

Influence of Blood-Pool Contrast Media on MR Imaging and Flow Measurements in the Presence of Pulmonary Arterial Stents in Swine[1]

PURPOSE: To compare the effects of various stents on magnetic resonance (MR) imaging flow volume measurements and to determine the value of a blood-pool MR imaging contrast medium in assessment of vascular stents.

MATERIALS AND METHODS: In 11 pigs, six nitinol stents (Memotherm), four platinum stents (NuMed), and one elgiloy stent (Wallstent) were placed in the main pulmonary artery under x-ray fluoroscopic guidance. MR imaging was performed 3 months after stent placement before and after injection of NC100150 contrast medium. Blood flow volumes were assessed with velocity-encoded cine MR imaging through and next to the stent. The signal-to-noise ratio and width of susceptibility artifacts of the stents also were determined. Measurements were analyzed with the paired Student *t* test and Bland-Altman test, where appropriate.

RESULTS: Blood flow volumes measured through the nitinol and platinum stents disclosed no significant difference between velocity-encoded cine MR imaging measurements through and next to the stent. On cine MR images, small susceptibility artifacts were observed around the nitinol and platinum stents. Signal-to-noise ratio in the stent lumen was reduced in nitinol and platinum stents when compared with that next to the stent. The elgiloy stent produced severe susceptibility artifacts, making measurement of flow volumes impossible. NC100150 injection caused no significant effect on flow volume measurements. It improved the signal-to-noise ratio of the pulmonary arterial lumen outside and, to a lesser extent, inside the stent.

CONCLUSION: Assessment of morphology and flow volumes through nitinol and platinum stents is feasible with MR imaging. Blood-pool contrast media provide persistent signal enhancement in the pulmonary artery and, to a lesser extent, in the lumina of nitinol and platinum stents.

Endovascular stents have been used increasingly during the past decades for treatment of patients with vascular obstruction, dissection, or aneurysm (1–4). During this period, magnetic resonance (MR) angiography and velocity-encoded cine (VEC) MR imaging have become established techniques for noninvasive assessment of the cardiovascular system (5–8). However, application of contrast material–enhanced and VEC MR imaging for assessment of stent patency and flow through stents has been limited.

Susceptibility artifacts at the stent wall and radio-frequency (RF) shielding effects inside the stent lumen can be misinterpreted as stent obstruction or occlusion (9–13). Moreover, quantitative assessment of blood flow through endovascular stents by using VEC MR imaging is considered to be problematic because of phase offset phenomena associated with magnetic susceptibility. Investigators in an in vitro study (14) to determine the accuracy of VEC MR imaging measurements in the presence of a stainless steel coronary

stent demonstrated significant decrease in flow velocity when it was measured near the stent. Several recent studies (15,16) have focused on characterization of the effect of a variety of stents at MR imaging and contrast-enhanced MR angiography. In these studies, readable MR images were obtained for some MR imaging–compatible stent materials and designs in conjunction with optimal sequence parameters such as short echo times and high flip angles.

Moreover, administration of extracellular gadolinium chelates was reported to improve MR imaging signal intensity inside the stent lumen (17). On the other hand, the value of blood-pool (intravascular) contrast agents in MR imaging of stents has not, to our knowledge, been evaluated. Blood-pool contrast agents allow prolonged delineation of central and peripheral vasculature and can provide greater signal-to-noise ratio (SNR) than can extracellular gadolinium chelates (18,19). Tello et al (20) demonstrated in eight patients the ability of first-pass gadopentetate dimeglumine in depicting the patency of stents placed in renal and iliac arteries.

The current study was designed to determine the effect of three stent types on VEC MR imaging and fast segmented cine MR imaging in an in vivo animal model. The potential beneficial effect of a blood-pool contrast medium also was evaluated. Specific aims were *(a)* to determine the accuracy of quantitative flow volume measurements through various types of endovascular stents, *(b)* to compare the effect of magnetic susceptibility and RF shielding on MR imaging in vivo, and *(c)* to evaluate effects of blood-pool contrast media on quantitative flow volume measurements, magnetic susceptibility, and RF shielding effects by using steady-state distribution of the contrast media.

MATERIALS AND METHODS

Stent Characteristics

Stents evaluated were six nitinol (Memotherm; Angiomed, Germany), four platinum (NuMed, New York, NY), and one elgiloy (Wallstent; Schneider, Bäulach, Switzerland) stent. NuMed stents consist of welded platinum wires, yielding a dimensionless susceptibility of 279×10^{-6}. This stent was balloon expanded to a diameter of 18 mm and a length of 17 mm. Memotherm stents consist of a laser-cut metal alloy composed of 50% titanium and 50% nickel (nitinol), yielding a susceptibility of -7×10^{-6} to -11×10^{-6}. This self-expanding stent is 18 mm in diameter and 25 mm long when fully expanded. The Wallstent is fabricated from a woven cobalt alloy (elgiloy), yielding a susceptibility of approximately 250×10^{-3}. The stent is self-expanding and has a diameter of 15 mm and a length of 20 mm when fully expanded.

Blood-Pool MR Imaging Contrast Medium (NC100150 Injection)

This blood-pool contrast agent (Clariscan; Nycomed Amersham, Oslo, Norway) is composed of single crystals with diameters of 4–7 nm and is stabilized with a carbohydrate polyethylene glycol. The iron oxide particles (particle concentration, 0.5%–1.0% weight/volume) were suspended in an isotonic glucose solution. The final diameter of the NC100150 injection is approximately 20 nm. The longitudinal relaxation rate of the agent is approximately 20 mmol/L/sec, and the transverse relaxation rate is 35 mmol/L/sec at 37°C and 0.5 T. Injection of NC100150 reduces blood T1 to less than 100 msec. Iron oxide particles are considered blood-pool agents, since their plasma half-life is 90 minutes in humans. In clinical trials now being conducted in the United States and Europe, ultrasmall superparamagnetic iron oxide, or USPIO, particles have been well tolerated in humans (21,22). USPIO particles represented by NC100150 injection have been successfully used for MR angiography of peripheral and pulmonary vessels and for three-dimensional cardiac cine MR imaging (23–26). The agent was obtained as a septum-sealed vial containing 10 mg iron per milliliter.

Study Design

All procedures were performed in accordance with the National Institute of Health guidelines for care and use of laboratory animals and with approval of the committee of animal research of the University of California, San Francisco. In 11 female farm pigs (mean body weight, 14.1 kg ± 1.5; Pork Power Farms, Turleck, Calif), endovascular stents were placed in the main pulmonary artery by using a transcatheter technique under x-ray fluoroscopic guidance (T.K., K.G., D.T., P.M.). Cine angiography was performed to verify the stent position. Postcatheterization treatment included oral administration of 250 mg/kg per day cephalosporin (Suprax; Wyeth-Ayerst, Philadelphia, Pa) over 1 week and 80 mg per day aspirin over the entire study.

The animals were studied with MR imaging 3 months after stent implantation. At this time, the weight of the animals had increased to 33 kg ± 2.3. Imaging was performed before and after intravenous injection of 0.05 mmol iron per kilogram NC100150. For all procedures, the animals were intramuscularly injected with a mixture of 0.025 mg/kg telazol (Telazol; Wildlife Pharmaceuticals, Fort Collins, Colo), ketamine hydrochloride (Ketaset; Fort Dodge Laboratories, Fort Dodge, Iowa), and xylazine hydrochloride (Anased; Lloyd Laboratories, Shenandoah, Iowa) for induction of and 2% isoflurane (Isoflo; Abbott Laboratories, North Chicago, Ill) inhalation for maintenance of general anesthesia. After completion of the MR imaging study, the animals were euthanized with 200 mg/kg intravenously administered sodium pentobarbital (Nembutal Sodium Solution; Abbott Laboratories). The heart was excised to evaluate the position and morphology of the stent and pulmonary artery. Stent placement was successful in all 11 animals. The stents were well tolerated, without complications or migration, over the 3-month period.

MR Imaging

Flow volume measurements.—MR imaging was performed by using a 1.5-T imager (Signa 5; GE Medical Systems, Milwaukee, Wis) with a standard body coil. All MR images were acquired with electrocardiographic gating. The positions of the main pulmonary artery and stent were identified with a set of scout images in sagittal and transverse planes.

VEC MR imaging sequence.—This MR imaging sequence was used to quantify pulmonary blood flow volumes through and next to the stent (27–29). All VEC MR imaging measurements were made in a double oblique plane perpendicular to the dominant flow direction in the main pulmonary artery. The distance between any visible stent artifact and the site of VEC MR imaging measurements next to the stent was chosen to be greater than 10 mm. Measurement errors due to the stent artifact were not expected at this distance. The effect of surgery on flow volume measurements has been addressed in control animals in our previous publication (30).

For VEC MR imaging measurements next to the stent, velocity maps were obtained by manually tracing the main pulmonary artery cross-sectional area on the

magnitude images and then applying it to the phase images (T.K., M.S.). For VEC MR imaging measurements through the stent, the contour of the stent was traced on both VEC magnitude images and VEC phase images, since the phase images showed less susceptibility artifact. Flow volume measurements of both methods for tracing the contour area were compared. There was a 1.0% ± 3.6 difference between the two methods, and these measurements were not significantly different. However, definition of the stent wall was found to be more unequivocal on VEC phase images; therefore, it was used in the calculation of flow volume measurements.

Flow volumes were calculated by multiplying cross-sectional area and spatial average flow velocity within the contour. Instantaneous flow volumes were summed to obtain the total flow volume per cardiac cycle. The following acquisition parameters were used for VEC MR imaging: repetition time msec/echo time msec, 25/7; section thickness, 5 mm; flip angle, 30°; receiver bandwidth, 31.25 kHz; field of view, 24 × 24 cm; matrix, 256 × 192; number of signals acquired, two; velocity-encoding gradient, 200 cm/sec. The average acquisition time was 3.19 minutes.

Cine MR imaging sequence.—This sequence was used to determine right ventricular stroke volumes (31–33). End-systolic and end-diastolic volume images were measured by manually tracing the area of the endocardial surfaces (T.K., M.S.). Ventricular chamber volumes were computed as the sum of right ventricular volumes of all short axis view sections containing right ventricular chambers. The area of each section was multiplied by section thickness to determine the volume of each level. Stroke volume was calculated as the difference between end-diastolic and end-systolic volumes. The following imaging parameters were used for cine MR imaging: 8/3; section thickness, 10 mm; spacing, 0; flip angle, 20°; receiver bandwidth, 31.25 kHz; field of view, 24 × 24 cm; matrix, 256 × 128; number of phases, 16; acquisition time, 4.17 minutes. Seven to ten sections were acquired to encompass the entire right ventricle.

Magnetic susceptibility and RF shielding.—The effects of susceptibility and RF shielding were analyzed quantitatively on VEC MR images acquired perpendicular to and on cine MR images acquired parallel to the long axis of the stent. All VEC and cine MR imaging was performed through the center portion of the stent. Susceptibility artifacts at the stent wall were measured as the number of pixels yielding total signal void. The degree of RF shielding was determined by comparing the MR imaging signal intensity measured in the center portion of the stent lumen with measurements obtained in the center of the pulmonary artery next to the stent (>10 mm) (T.K., M.S.).

In general, the surface area of the examined vessel (without stents) is traced on magnitude images from VEC MR imaging. In this study, however, we measured flow volumes through endovascular stents. It is well known that metallic stents produce different degrees of artifacts on MR images. We found that on magnitude images artifacts were relatively large and superimposing the vessel wall. This made unequivocal delineation of the wall difficult. On phase images, stent artifacts were relatively smaller than on magnitude images. Therefore, unequivocal delineation of the vessel wall was relatively easier. In the current study, we compared the two methods of tracing the vessel wall (once on the magnitude and once on the phase images). We found that the difference in flow volume measurements was 1.0% ± 3.6 (P = not significant; paired Student t test) between the two methods of tracing in the nitinol and platinum stents.

The rationales for examining the susceptibility and RF shielding effects of each stent on flow were: *(a)* The differences in the alloy of these stents cause different degrees of shielding effects, and *(b)* the magnitude of susceptibility artifact g is dependent on the material properties of the stent.

Influence of blood-pool contrast medium on cine and VEC MR imaging.—To assess the effects of blood-pool contrast media on cine and VEC MR images during steady-state distribution, measurements of pulmonary flow volumes, SNR, and artifact width were repeated after intravenous injection of 0.05 mmol iron per kilogram NC100150 (M.S., T.K.). All measurements were completed within 30 minutes after administration of the contrast agent.

Statistical Analysis

Data are presented as mean ± SD. The unpaired Student t test and analysis of variance were used to determine differences between animals with different stents. The paired Student t test was applied for comparison of measurements within the same animal. A P value of less than .05 was considered to indicate a significant difference. Linear regression analysis with calculation of SDs was used to determine correlation between pulmonary flow volume measurements assessed with VEC MR imaging through and next to the stent. In addition, the Bland-Altman test was performed to determine agreement between pulmonary flow volumes as measured with VEC MR imaging through and next to the stent and with cine MR imaging.

RESULTS

At autopsy, partial endothelialization without significant intimal hyperplasia was noted at the stent wall.

Effects of Various Stents on Flow Volume Measurements

The elgiloy stent (Wallstent) caused susceptibility artifacts at the implantation site that prohibited visualization of underlying structures (Fig 1). Therefore, measurement of pulmonary blood flow in or next to this stent was not possible due to susceptibility artifacts.

Measurement of pulmonary flow volumes within nitinol (Memotherm) and platinum (NuMed) stents showed no significant differences between VEC MR imaging measurements through and next to the stents (Table 1). As compared with flow volume measurements next to the stents, flow volumes through the nitinol stents were underestimated by 8% ± 8 (P = not significant, paired Student t test) and by 2% ± 7 (P = not significant, paired Student t test) when measured through the platinum stents. Correlation coefficients between VEC MR imaging measurements through and next to the stents were excellent for both the nitinol and platinum stents (r = 0.96, $P < .05$ and r = 0.93, $P < .05$). Excellent agreement was found between VEC MR imaging measurements next to and through the nitinol and platinum stents with the Bland-Altman test.

As compared with right ventricular stroke volume measurements obtained with cine MR imaging (2,547 mL ± 290), VEC MR imaging flow volumes (2,417 mL ± 419) were underestimated by 5% ± 6 (P = not significant, paired Student t test) when measured through the nitinol stents. As compared with right ventricular stroke volume measurements obtained with cine MR imaging (2,381 mL ± 354), VEC MR imaging flow volumes (2,294 mL ± 348) were underestimated by 4% ± 5 (P = not significant, paired Student t test) when measured through the platinum stents. Excellent

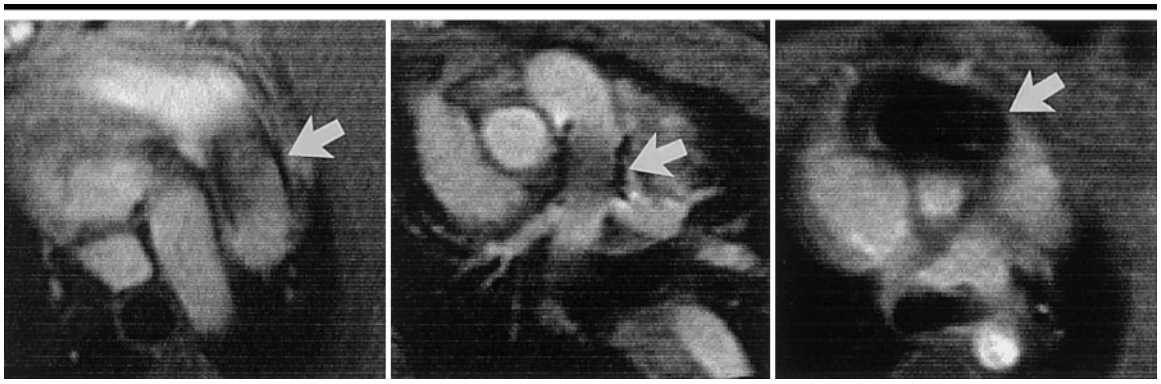

Figure 1. Cine MR images (8/3; flip angle, 20°; section thickness, 10 mm) acquired through longitudinal midportion of Memotherm nitinol stent (left), NuMed platinum stent (center), and elgiloy Wallstent (right) 3 months after stent placement in main pulmonary artery. Susceptibility artifacts (arrow) were less pronounced with nitinol and platinum stents and were severe with Wallstents, which caused severe image distortion due to the artifacts.

agreement was found between pulmonary flow volumes measured with VEC MR imaging and right ventricular stroke volumes measured with cine MR imaging for nitinol and platinum stents by using the Bland-Altman test.

TABLE 1
Effect of Different Stent Types and NC100150 Injection on VEC MR Imaging Flow Volume Measurements

Stent Type and Contrast Medium	Mean Flow Volume (mL/min)	
	Through Stent	Next to Stent
Nitinol (Memotherm)		
No contrast medium	2,417 ± 219	2,619 ± 368
NC100150	2,276 ± 210	2,554 ± 104
Platinum (NuMed)		
No contrast medium	2,294 ± 248	2,351 ± 234
NC100150	2,123 ± 177	2,530 ± 287
Elgiloy (Wallstent)		
No contrast medium	Not available	2,213 ± 202
NC100150	Not available	2,144 ± 319

Appearance of Various Stents at MR Imaging

Image analysis for the elgiloy stent was not feasible due to severe susceptibility artifacts extending from the stent wall over the entire lumen and beyond the border of the stent on VEC and cine MR images. In the nitinol and platinum stents, circular margins were well defined on VEC phase images (Fig 2). In the nitinol stents, a ring of artifact 1 pixel ± 0.4 wide was noted. For the platinum stents, the artifact width was 1.1 pixels ± 0.8. In contrast, VEC magnitude images showed greater susceptibility artifacts extending over 3.9 pixels ± 0.8 in the nitinol stent and 4.1 pixels ± 0.6 in the platinum stent. The artifacts on the magnitude images prevented accurate identification of the contour and dimensions of the stent.

On cine MR images, susceptibility artifacts of the nitinol and platinum stents did not cause major image distortion (Fig 1). The artifact width was 2.8 pixels ± 0.4 for the nitinol stent and 3.2 pixels ± 0.5 for the platinum stent. This relatively small artifact size allowed good delineation of the pulmonary artery, definition of the stent position in the vessel (Fig 3), and definition of the stent lumen. SNR measured inside the stent lumen was significantly ($P < .01$) reduced for both the nitinol and platinum stents when compared with measurements obtained next to the stent (Table 2). Reduction of SNR inside the stent lumen was 55% ± 8 (from 8.5% ± 2.2 to 3.8% ± 0.4) for the nitinol stent and 42% ± 10 (from 4.3% ± 3.2 to 5.4% ± 0.6) for the platinum stent.

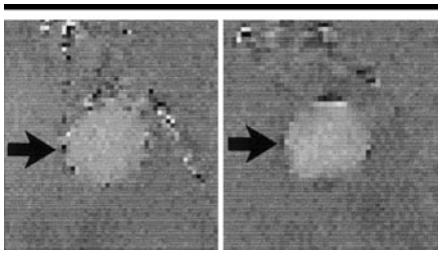

Figure 2. VEC MR imaging phase images (25/7; flip angle, 30°; section thickness, 5 mm) acquired during midsystole through Memotherm nitinol (left) and NuMed platinum (right) stents. Circular margin of the stents is well defined. The stents produced very small artifacts not exceeding a width of 2 pixels (arrow). Flow phenomena are visible over the entire stent lumina.

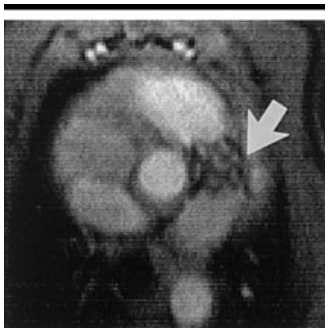

Figure 3. Cine MR image (8/3; flip angle, 20°; section thickness, 10 mm) acquired through wall of platinum stent clearly depicts stent morphology (arrow), including structures of wire mesh and surrounding tissue.

Influence of NC100150 Injection on MR Imaging Flow Volume and MR Imaging

Injection of NC100150 increased the MR imaging signal intensity of the blood pool outside and inside the nitinol and platinum stents (Table 2, Fig 4). SNR measured in the pulmonary artery outside the stents was increased by 76% ± 7 ($P < .01$) with NC100150 injection. However, the contrast media increased SNR slightly but significantly ($P < .05$) inside the stent lumen. The increase was 17% ±

TABLE 2
Effect of NC100150 Injection on Appearance of Endovascular Stents on Cine MR Images

Stent Type and Contrast Medium	Susceptibility Artifact Width (pixels)	SNR	
		Inside Stent	Next to Stent
Nitinol (Memotherm)			
No contrast medium	2.8 ± 0.4	3.8 ± 0.4	8.5 ± 2.2
NC100150	2.9 ± 0.6	4.6 ± 0.5	38.3 ± 3.9
Platinum (NuMed)			
No contrast medium	3.2 ± 0.5	5.4 ± 0.6	9.3 ± 3.2
NC100150	3.1 ± 0.6	6.9 ± 1.1	35.9 ± 4.2
Elgiloy (Wallstent)			
No contrast medium	>10.0	Not available	9.1 ± 0.8
NC100150	Not available	Not available	Not available

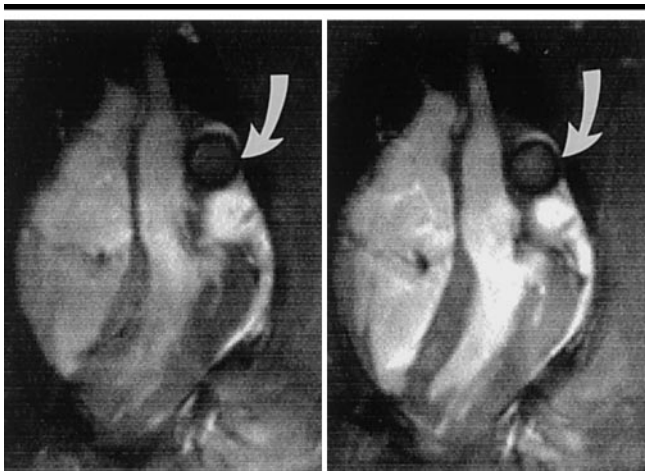

Figure 4. VEC MR magnitude image (25/7; flip angle, 30°; section thickness, 5 mm) acquired through midportion of nitinol stent (arrow) in pulmonary position during midsystole before (left) and 20 minutes after (right) administration of 0.05 mmol iron per kilogram blood-pool MR imaging contrast medium NC100150. Contrast medium enhanced SNR in cardiac chambers, ascending aorta, and pulmonary vasculature and to a lesser extent in stent lumen.

9 in the nitinol stent and 23% ± 9 in the platinum stent. Absolute SNR data are shown in Table 2. The signs of susceptibility artifacts of the stent were not influenced by injection of NC100150 (Table 2).

The MR imaging contrast agent did not cause any significant effect on flow volume measurements or cardiac output. Differences between flow volume measurements without and with NC100150 injection ranged from 5% ± 9 to 7% ± 8 when measured through the stent and from 2% ± 8 to 7% ± 11 when measured next to the stent (Table 1).

DISCUSSION

Results of the current study imply that MR imaging is an effective and noninvasive method to quantify blood flow through endovascular platinum and nitinol stents and to assess stent morphology. Because of the ability to provide quantitative flow information and images with high soft-tissue contrast in any orientation, MR imaging seems well suited to monitor stent patency and detect hemodynamically significant stenosis in patients with stents in peripheral and central vascular positions.

The accuracy of MR imaging to quantify vascular blood flow has been validated in several studies (27–29). However, the question of whether flow measurements are feasible after stent placement has not, to our knowledge, been answered. Because magnetic susceptibility results in intravoxel spin dephasing, phase-contrast sequences used for blood flow measurements may be especially prone to phase offset errors. One specific aim of this study was to evaluate the effect of different stent types on VEC MR imaging measurements in situ. Results of the current study show that flow volume measurements are reasonably accurate when obtained inside stents with relatively low magnetic susceptibility and large surface areas. On the other hand, flow measurements obtained through stents with high magnetic susceptibility, such as elgiloy stents, were not feasible. These findings imply that phase errors caused by local field inhomogeneities around nitinol and platinum stents are limited to areas adjacent to the stent wall and do not significantly affect flow measurements through stents with large diameters. In further research, pulse sequences with short echo times or refocusing pulses should be investigated to reduce intravoxel spin dephasing and thus to minimize errors in quantitative flow measurements. By using such pulse sequences, noninvasive MR imaging evaluation of stent patency in small vessels such as the coronary arteries might become feasible.

One major problem in MR imaging of endovascular stents is susceptibility artifacts (34,35). Susceptibility artifacts cause phase and frequency offset phenomena leading to image distortion at the stent wall. The extent of the artifact depends on several factors including but not limited to material properties, gradient field strength, orientation of the stent toward the main magnetic field, and imaging parameters such as echo time and receiver bandwidth. In the current study, MR imaging of elgiloy stents (Wallstents), which are fabricated from a strongly magnetic alloy, showed severe susceptibility artifacts, which prevented appropriate definition of stent wall and lumen patency. In contrast, magnetic susceptibility values of nitinol (Memotherm) and platinum (NuMed) stents are relatively close to those of human tissue. In the current study, both stent types yielded very similar sizes of susceptibility artifacts. On cine MR images, artifact size was relatively small and allowed precise definition of stent morphology and position in the pulmonary artery. On images obtained through the walls of nitinol and platinum stents, the structure of the wire mesh was distinguishable from surrounding tissue. This suggests the possibility that stent obstruction by tissue proliferation might be directly visualized on MR images when using appropriate imaging sequences and stent designs.

Differences in artifact sizes of stents on cine and VEC MR magnitude images are presumably due to differences in the echo times of the two MR imaging se-

quences (3 and 7 msec, respectively). On VEC phase images, signs of artifacts were even less pronounced than on cine MR images, although longer echo times were used. A possible explanation is that velocity maps compensate for spin frequency offset phenomena, which are caused by local field inhomogeneities due to susceptibility.

Another problem in MR imaging of endovascular stents is the RF (B_1-field) shielding effect (36). RF pulses induce electrical eddy currents in closed loops of the stent mesh and thus magnetic flux. The main component of the magnetic flux opposes the originating RF field. Consequently, flip-angle excitation inside the stent lumen is reduced, leading to poor SNR. The amount of shielding depends mainly on the design of the stent mesh, stent geometry (eg, length), orientation of the stent toward the RF pulse direction, and sequence parameters such as flip angle. Stents designed with few or no conducting closed loops would avoid electrical flow of eddy currents (37).

In the current study, differences in SNR were found when measured inside the lumina of platinum and nitinol stents. One obvious difference between the nitinol and platinum stents was length (17 and 25 mm, respectively). Penetration of RF pulses through the open cross-sectional ends of a stent may be one important source for improving intraluminal SNR. Thus, short stents may benefit from this mechanism more than long stents.

There were three reasons for using the blood-pool MR imaging contrast medium: *(a)* to determine the effect of this blood-pool agent on flow volume measurement, *(b)* to improve contrast between blood in the left ventricular chamber and in myocardium on cine MR images, and *(c)* to visualize the patency of the stents after deployment. In the current study, injection of NC100150 improved image quality in the stent lumen slightly but significantly. However, this contrast agent clearly enhanced the contrast between the endovascular stent, vascular blood pool, and surrounding tissue. Lack of substantial enhancement of the stent lumen after shortening of blood T1 is most likely related to the RF shielding effects produced by all of the stents used in the current study. NC100150 injection enabled persistent and excellent delineation of central pulmonary vasculature for at least 30 minutes. In addition, the contrast media did not have any significant effects on VEC MR imaging flow volume measurements.

Bolus administration of the extracellular MR imaging contrast medium gadopentetate dimeglumine has been previously used to assess the patency of endovascular stents placed in the renal and iliac arteries in patients (20). In the current study, in contrast with previous first-pass studies (20), NC100150 injection was used to detect patency of the pulmonary artery by using the steady-state distribution approach of the contrast medium. An advantage of this approach is that MR imaging can be performed in a wide time window (approximately 30 minutes) after injection. It was anticipated that the contrast medium would have no effect on cardiac output.

Authors of recently published reports (38–42) have documented the feasibility of MR imaging not only to detect vascular obstruction but also to guide angioplasty and endovascular stent placement for their treatment. High and persistent contrast between the vascular blood pool and endovascular devices, as achieved with NC100150 injection, might be of importance for visualizing stent patency and when using interventional MR imaging techniques for treatment of vascular obstruction or after deployment of endovascular stents. VEC MR imaging flow measurements before and after stent placement could then be used for documentation of the effectiveness of the procedure and for noninvasive follow up.

Practical application: Appropriate imaging sequences and stent types are crucial factors for noninvasive assessment of endovascular stents with MR imaging. Quantitative blood flow measurements with VEC MR imaging and use of blood-pool MR imaging contrast media are promising methods for accurate assessment of stent morphology and patency.

References

1. Dolmatch BL, Blum U. Stent-grafts: current clinical practice. New York, NY: Thieme, 2000.
2. Blum U, Langer M, Spillner G, et al. Abdominal aortic aneurysms: preliminary technical and clinical results with transfemoral placement of endovascular self-expanding stent graft. Radiology 1996; 198:25–31.
3. Gragg A, Dake M. Treatment of peripheral vascular disease with stent-grafts. Radiology 1997; 25:74–83.
4. Cheung YF, Sanatani S, Leung MP, et al. Early and intermediate-term complications of self-expanding stents limit its potential application in children with congenital heart disease. J Am Coll Cardiol 2000; 35:1007–1015.
5. Hany TF, McKinnon GC, Leung DA, et al. Optimization of contrast timing for breath-hold three dimensional MR angiography. J Magn Reson Imaging 1997; 7:551–556.
6. Edelmann RR. MR angiography: present and future. AJR Am J Roentgenol 1993; 161:1–11.
7. Yucel EK, Silver MS, Carter AP. MR angiography of normal pelvic arteries: comparison of signal intensity and contrast-to-noise ratio for three different inflow techniques. AJR Am J Roentgenol 1994; 163:197–201.
8. Haussmann R, Lewin JS, Laub G. Phase contrast MR angiography with reduced acquisition time: new concepts in sequence design. J Magn Reson Imaging 1991; 1:415–422.
9. Vorwerk D, Günther RW, Schürmann K, et al. Aortic and iliac stenoses: follow-up results of stent placement after insufficient balloon angioplasty in 118 cases. Radiology 1996; 198:45–48.
10. Hilfiker PR, Quick HH, Debatin JF. Plain and covered stent-grafts: in vitro evaluation of characteristics at three-dimensional MR angiography. Radiology 1999; 211:693–697.
11. Hilfiker PR, Quick HH, Pfammatter T, et al. Three-dimensional MR angiography of a nitinol-based abdominal aortic stent graft: assessment of heating and imaging characteristics. Eur Radiol 1999; 9:1775–1780.
12. Duerinckx AJ, Atkinson D, Hurwitz R. Assessment of coronary artery patency after stent placement using magnetic resonance angiography. J Magn Reson Imaging 1998; 8:896–902.
13. Link J, Steffens J, Brossmann J, et al. Iliofemoral arterial occlusive disease: contrast-enhanced MR angiography for preinterventional evaluation and follow-up after stent placement. Radiology 1999; 212:371–377.
14. Lethimonnier F, Bouligand B, Thouveny F, et al. Error assessment due to coronary stents in flow-encoded phase contrast MR angiography: a phantom study. J Magn Reson Imaging 1999; 10:899–902.
15. Klemm T, Duda S, Machann J, et al. MR imaging in the presence of vascular stents: a systematic assessment of artifact for various stent orientations, sequence types, and field strengths. J Magn Reson Imaging 2000; 12:606–615.
16. Lehnhart M, Voelk M, Nitz WR, et al. Stent appearance at contrast-enhanced MR angiography: in vitro examination with 14 stents. Radiology 2000; 217:173–178.
17. Matsumoto AH, Teitelbaum GP, Carvlin MJ, et al. Gadolinium enhanced MR imaging of vascular stents. J Comput Assist Tomogr 1990; 14:357–361.
18. Kellar KE, Fujii DK, Gunther WHH, et al. NC100150 injection, a preparation of optimized iron oxide nanoparticles for positive-contrast MR angiography. J Magn Reson Imaging 2000; 11:488–494.
19. Anzai Y, Prince MR, Chenevert TL, et al. MR angiography with an ultrasmall superparamagnetic iron oxide blood pool agent. J Magn Reson Imaging 1997; 7:209–214.
20. Tello R, Thomson KR, Witte D, Becker GJ, Tress BM. Dynamic gadolinium DTPA-enhanced magnetic resonance of intravascular stents. Invest Radiol 1998; 33:411–414.

21. Panting JR, Taylor AM, Gatehouse PD, et al. First-pass myocardial perfusion imaging and equilibrium signal changes using the intravascular contrast agent NC100150 injection. J Magn Reson Imaging 1999; 10:404–410.
22. Taylor AM, Panting JR, Keegan J, et al. Safety and preliminary findings with the intravascular contrast agent NC100150 injection for MR coronary angiography. J Magn Reson Imaging 1999; 9:220–227.
23. Amano Y, Herfkens RJ, Shifrin RY, et al. Three-dimensional cardiac cine magnetic resonance imaging with an ultrasmall superparamagnetic iron oxide blood pool agent (NC100150). J Magn Reson Imaging 2000; 11:81–86.
24. Bremerich J, Roberts TPL, Wendland MF, et al. Three-dimensional MR imaging of pulmonary vessels and parenchyma with NC100150 injection (Clariscan). J Magn Reson Imaging 2000; 11:622–628.
25. Saeed M, Wendland MF, Engelbrecht M, et al. Value of blood pool contrast agents in magnetic resonance angiography of the pelvis and lower extremities. Eur Radiol 1998; 8:1047–1053.
26. Stillmann AE, Wilke N, Li D, et al. Ultrasmall superparamagnetic iron oxide to enhance MRA of the renal and coronary arteries: studies in human patients. J Comput Assist Tomogr 1996; 20:51–55.
27. Rehbergen SA, Chin JGJ, Ottenkamp J. Pulmonary regurgitation in the late postoperative follow-up of tetralogy of Fallot. Circulation 1993; 88:2257–2266.
28. Mostbeck GH, Caputo GR, Higgins CB. MR measurement of blood flow in the cardiovascular system. AJR Am J Roentgenol 1992; 159:453–463.
29. Gutberlet M, Boeckel T, Hosten N, et al. Arterial switch procedure for D-transposition of the great arteries: quantitative midterm evaluation of hemodynamic changes with cine MR imaging and phase-shift velocity mapping—initial experience. Radiology 2000; 214:467–475.
30. Kuehne T, Saeed M, Reddy G, et al. Sequential MR monitoring of pulmonary flow with endovascular stents placed across the pulmonary valve in growing swine. Circulation 2001; 104:2362–2368.
31. Rominger MB, Bachmann GF, Pabst W, et al. Right ventricular volumes and ejection fraction with fast cine MR imaging in breath-hold technique: applicability, normal values from 52 volunteers, and evaluation of 325 adult cardiac patients. J Magn Reson Imaging 1999; 10:908–918.
32. Pattynama PMT, Lamb HJ, Van der Velde EA, et al. Reproducibility of MRI-derived measurements of right ventricular volumes and myocardial mass. Magn Reson Imaging 1995; 13:53–63.
33. Pattynama PMT, de Roos A, van der Wall E, et al. Evaluation of cardiac function with magnetic resonance imaging. Am Heart J 1994; 128:595–607.
34. Schenck JF. The role of magnetic susceptibility in magnetic resonance imaging: magnetic compatibility of the first and second kinds. Med Phys 1996; 23:815–851.
35. Teitelbaum GP, Bradley WG, Klein BD, et al. MR imaging artifacts, ferromagnetism, and magnetic torque of intravascular filters, stents and coils. Radiology 1988; 166:657–664.
36. Haacke EM, Brown RW, Thompson MR, et al. Magnetic resonance imaging: physical principles and sequence design. New York, NY: Wiley, 1999.
37. Ozaki Y, Violaris AG, Serruys PW. New stent technologies. Prog Cardiovasc Dis 1996; 39:129–140.
38. Ladd ME, Quick HH, Debatin JF, et al. Interventional MRA and intravascular imaging. J Magn Reson Imaging 2000; 12: 534–546.
39. Buecker A, Neuerburg M, Adam GB, et al. Real-time fluoroscopy for MR-guided iliac artery stent placement. J Magn Reson Imaging 2000; 12:616–622.
40. Yang X, Bolster BD, Kraitchman DL, et al. Intravascular MR-monitored balloon angioplasty: an in-vivo feasibility study. J Vasc Interv Radiol 1999; 9:952–959.
41. Engellau L, Olsrud J, Brockstedt S, et al. MR evaluation ex vivo and in vivo of a covered stent-graft for abdominal aortic aneurysms: ferromagnetism, heating, artifacts and velocity mapping. J Magn Reson Imaging 2000; 12:112–121.
42. Dion YM, El Kadi H, Boudoux C, et al. Endovascular procedures under near real-time magnetic resonance imaging guidance: an experimental feasibility study. J Vasc Surg 2000; 32:1006–1014.